# Interpretation of heterogeneity effects in synchrotron X-ray fluorescence microprobe data

**Mavrik Zavarin*[a] and Harvey E. Doner[b]**

[a]*Lawrence Livermore National Laboratory, 7000 East Avenue, L-221 Livermore, USA. E-mail: zavarin1@llnl.gov*
[b]*University of California at Berkeley, 151 Hilgard Hall, Berkeley, USA. E-mail: doner@nature.berkeley.edu*

**Article**

***Received 8th May 2002, Accepted 25th July 2002***
***Published on the Web 20th August 2002***

Heterogeneity effects often limit the accuracy of synchrotron X-ray fluorescence microprobe elemental analysis data to ±30%. The difference in matrix mass absorption at Kα and Kβ fluorescence energies of a particular element can be exploited to yield information on the average depth-position of the element or account for heterogeneity effects. Using this technique, the heterogeneous distribution of Cu in a simple layered sample could be resolved to a 2 × 2 × 10 ($x$, $y$, $z$, where $z$ is the depth coordinate) micrometer scale; a depth-resolution limit was determined for the first transition metal series and several other elements in calcite and iron oxide matrices. For complex heterogeneous systems, determination of average element depth may be computationally limited but the influence of heterogeneity on fluorescence data may still be assessed. We used this method to compare solid-state diffusion with sample heterogeneity across the Ni-serpentine/calcite boundary of a rock from Panoche Creek, California. We previously reported that Ni fluorescence data may indicate solid state diffusion; in fact, sample heterogeneity in the depth dimension can also explain the Ni fluorescence data. Depth heterogeneity in samples can lead to misinterpretation of synchrotron X-ray microprobe results unless care is taken to account for the influence of heterogeneity on fluorescence data.

## Introduction

A synchrotron X-ray fluorescence microprobe (SXRFM) has been in use at the National Synchrotron Light Source (NSLS), Brookhaven National Laboratory, since March 1986.[1] New higher flux third generation synchrotron X-ray sources such as the Advanced Photon Source (APS), Argonne National Laboratory, and several others have more recently become available for SXRFM studies. Due to the high brightness of these sources, elemental mapping can be accomplished at the sub-ppm level. In addition, focusing techniques (*e.g.* multilayer Kirkpatrick–Baez mirrors,[2,3] zone plates and tapered capillaries) can now reduce the beam to $< 1$ μm$^2$ spot sizes to achieve unprecedented spatial resolutions. Though techniques such as the electron microprobe, secondary ion mass spectrometry, and others may have similar spatial resolution or similar detection limits in some cases, one of the most appealing aspects of the SXRFM is that samples can be run at atmospheric pressures and temperatures which is particularly important for characterization of environmentally sensitive samples.[4] SXRFM can also provide information on element speciation when fluorescence is measured as a function of primary X-ray energy. These advantages make SXRFM an ideal tool for 2-D elemental mapping of environmental samples.

The use of SXRFM in the analysis of environmental samples has been particularly popular due to the low detection limits for environmentally significant elements and little sample treatment which reduces the possibility for sample preparation effects. Geological investigations have included trace element analysis of extraterrestrial materials, sediments, and fluid inclusions,[1,5] as well as oxidation state analysis of minerals.[6] SXRFM has also been used in quantification of various environmental problems such as radionuclide migration through sediments, redox-controlled mobility of toxic metals in soils, and plant–metal interactions.[7,8] However, due to the highly heterogeneous matrix that usually composes "real" environmental samples, precise quantification of metal concentrations is difficult, as will be discussed below.

In traditional XRF elemental analysis, the effect of sample heterogeneity on the apparent concentration of trace elements in a sample has been widely studied.[9–16] Though there have been many techniques that have improved the accuracy of traditional XRF elemental analysis (scattered radiation, internal standards, standard addition, dilution methods, several mathematical methods, and dual measurement methods),[17–22] most require sample homogenization and are, thus, inappropriate for 2-D elemental mapping. SXRFM encounters the same problem as XRF analysis; this typically limits SXRFM accuracy to ±30% in thick heterogeneous samples. The accuracy can be improved by ensuring relative homogeneity of the sample or by carefully choosing standards of similar composition to the unknown; ultimately, heterogeneity effects are best minimized by reducing sample thickness (typically to 10–30 μm) which drastically improves SXRFM accuracy.[1,23,24]

The basic behavior of the primary X-rays and fluorescence X-rays in a homogeneous and simple heterogenous sample is described in the Appendix. More detailed descriptions of X-ray interaction with homogeneous/heterogeneous samples can be found in other sources.[12,25] For a simple heterogeneous sample in which a trace element is buried within a matrix (equation derived in the Appendix),

$$I'_{\mathrm{L}}(\lambda_{\mathrm{s}}) = I_{\mathrm{L}}(\lambda_{\mathrm{s}})\mathrm{e}^{-\rho'_{\mathrm{f}} d(\mu'_{\mathrm{f}}(\lambda_{\mathrm{p}}) + \mu'_{\mathrm{f}}(\lambda_{\mathrm{s}}))} \quad (1)$$

where: $I'_{\mathrm{L}}(\lambda_{\mathrm{s}})$ is the fluorescence intensity from the buried trace element (cm$^{-2}$); $I_{\mathrm{L}}(\lambda_{\mathrm{s}})$ is the calculated homogeneous fluorescence intensity of the non-buried trace element (calculated in the Appendix); $\rho'_{\mathrm{f}}$ is the density of the overlying matrix (g cm$^{-3}$); $\mu'_{\mathrm{f}}(\lambda_{\mathrm{p}})$ and $\mu'_{\mathrm{f}}(\lambda_{\mathrm{s}})$ are the matrix mass absorption (cm$^2$ g$^{-1}$) for primary and fluorescent radiation, respectively; and $d$ is the thickness of the overlying matrix (cm). Since the Kα

and Kβ fluorescence lines for the same trace element have different energies, the mass absorption of X-rays at those energies ($\mu_f'(\lambda_s)$) will be different. It follows that the influence of depth-position on fluorescence intensity at the two X-ray energies will differ. It is this phenomenon that can be exploited to examine the heterogeneous distribution of a trace element in the depth dimension of a sample. Note that $I_L$, in fact, is also influenced by the difference in mass absorption at the Kα and Kβ energies; if the fluorescing element is a trace or minor component of the sample, the change in mass absorption as a function of concentration will be negligible. The method of using Kα and Kβ absorption differences was recently proposed by Phillippot *et al.*[26] as a means of correcting for mass aborption of host material during elemental analysis of fluid inclusions. Here, we discuss this method in terms of heterogeneity effect correction in geologic samples. The limitations of relating fluorescence intensity to relative concentration in heterogeneous samples are discussed and a means for rigorous interpretion of fluorescence data is described.

## Methods

### Synchrotron X-ray fluorescence microprobe set-up

Samples were run both at the Advanced Light Source (ALS), Lawrence Berkeley National Laboratory, microprobe beam line 10.3 (for Cu wedge and Panoche Creek samples) and NSLS beam line X26A (for Sn wedge samples). The ALS microprobe was configured with 10 keV multi-layer Kirkpatrick–Baez mirrors focused to 3 by 5 μm at the surface while the NSLS beam line was configured with slits set to approximately 50 by 50 μm. Beam spots as small as 25 $\mu m^2$ have been achieved using slits and pinholes at NSLS[27] while Kirkpatrick–Baez mirrors can reduce beam spots to 1 $\mu m^2$ or less.[2,3] Sample fluorescence was measured at 90° to the primary beam to reduce background radiation at the detector. Counting times per position were held between 10 and 20 seconds in all samples.

### Simple heterogeneous sample fluorescence experiments

Cu and Sn wedges were constructed to test sample heterogeneity behavior using simple model samples; Fig. 1 shows a cross section of the prepared sample. Cu or Sn wire was used to vapor deposit thin coats of metal onto one side of a polished limestone block and yield a metal coverage of approximately $10^{-5}$ g $cm^{-2}$. The 2 by 2 cm by 3 mm block of limestone was then mounted onto high-purity quartz round-mounts using standard geologic thin-sectioning adhesive resins. Finally, the limestone was shaped into a wedge using wheel sanders and polished with 0.25 μm diamond polish. The limestone had a grain size of approximately 5 μm and was composed mainly of Ca and Mg carbonate with some trace Fe.

### Ni heterogeneity analysis across a serpentine–calcite interface

A Ni-serpentine rock which had secondary calcite accumulations on its surface was collected from the Panoche Creek area of California. It was previously thought that the sample showed possible solid state diffusion of Ni from the serpentine to the overlain calcite.[28] The rock sample was sectioned and polished; the sample thickness was approximately 5 mm. The Ni concentration in the serpentine was 1500 mg $kg^{-1}$.

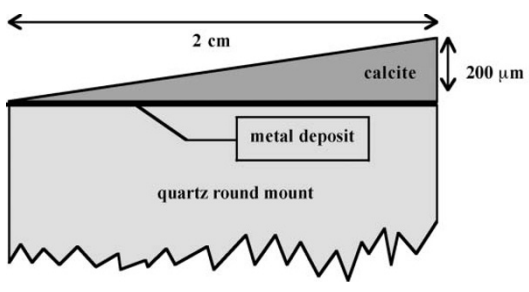


**Fig. 1** A diagram of the constructed limestone wedge.

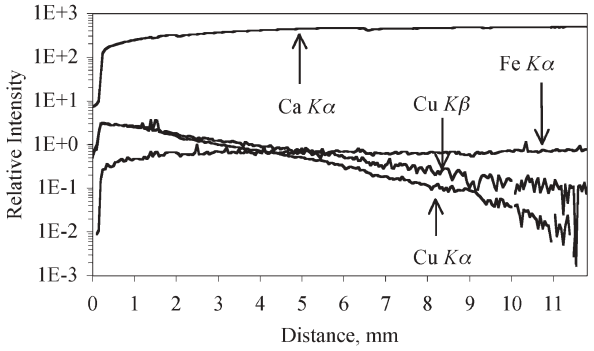


**Fig. 2** Ca Kα, Fe Kα, Cu Kα, and Cu Kβ fluorescence across a limestone wedge. The limestone overlayer thickness increases along the *x* axis.

## Results and discussion

Fig. 2 is a plot of fluorescence from a Cu-limestone wedge at Ca Kα, Fe Kα, Cu Kα, and Cu Kβ energies. The maximum limestone thickness in this sample is approximately 200 μm. While Ca Kα and Fe Kα fluorescence increases with increasing overlayer thickness, both Cu Kα and Cu Kβ fluorescence decreases. Furthermore, Cu Kα fluorescence decreases more rapidly than Cu Kβ fluorescence. The higher energy Cu Kβ fluorescence is less absorbed by the limestone than Cu Kα fluorescence. The observed linear relationship between overlayer thickness and ln(Kα/Kβ) fluorescence can be determined from first principles (shown later in eqn. 2).

Fig. 2 illustrates the effect of sample heterogeneity on quantitative analysis by SXRFM. The overlayer thickness drastically changes the apparent Cu concentration in the sample. In fact, the fluorescence signal varies by more than an order of magnitude across this sample. From Cu Kα fluorescence data alone, depth-heterogeneity and homogeneous changes in metal concentration cannot be distinguished. However, the Cu Kα and Kβ fluorescence signals are influenced by depth heterogeneity to different degrees; this relationship can be used to distinguish between variation in average Cu depth (heterogeneity) and homogeneous concentration changes.

A similar limestone wedge with vapor deposited Sn (Fig. 3) shows little variation in fluorescence across the limestone wedge because the mass absorption of the limestone at the Sn Kα and Kβ fluorescence energies is very low. Element depth variations of 200 μm do not significantly affect the fluorescence signal of the Sn Kα line. The depth resolution using the Kα/Kβ

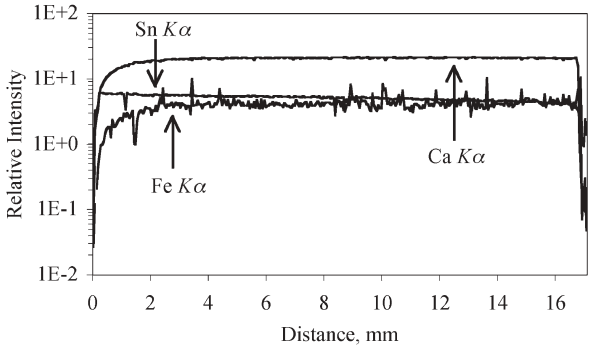


**Fig. 3** Ca Kα, Fe Kα, and Sn Kα fluorescence across a limestone wedge. The limestone overlayer thickness increases along the *x* axis.

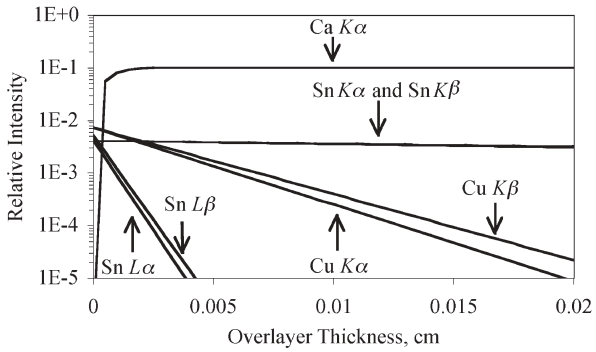


**Fig. 4** Model results for fluorescence of Ca Kα, Cu Kα, Cu Kβ, Sn Kα, Sn Kβ, Sn Lα, and Sn Lβ across a limestone wedge. The limestone overlayer thickness increases along the *x* axis.

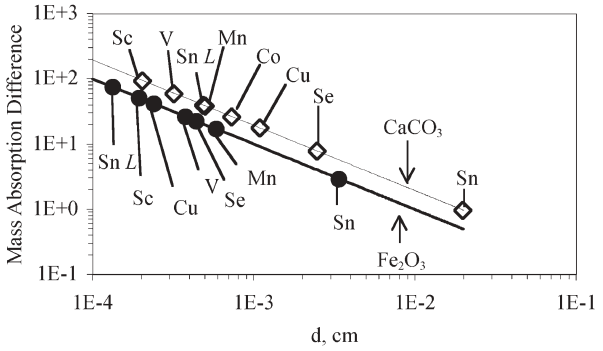


**Fig. 5** Curves predicting the attainable resolution for various elements in calcite and hematite matrices. All elements refer to mass absorption difference between Kα and Kβ energies except Sn L which refers to the mass absorption difference between Lα and Lβ energies.

ratio for this element and under these conditions will, therefore, be poorer.

Fig. 4 is a plot of results from model calculations that mimic the Cu and Sn deposited limestone wedge samples. The mass absorption values used in the model were derived from the empirical equations calculated by Wernisch *et al.*[29] from the published mass absorption tables of McMaster *et al.*[30] These results agree with experimental data (Figs. 2 and 3) indicating that the fluorescence ratio effect can be easily described using simple mass absorption equations. The model Sn Kα and Kβ fluorescence difference is unresolvable while the Cu Kα and Kβ difference is easily resolved within the 200 μm overlayer range. Included in this plot are Sn Lα and Lβ fluorescence; L-shell fluorescence will be affected in the same manner as K-shell fluorescence but the lower energy L-shell fluorescence will, generally, have a greater sensitivity to depth.

Figs. 2–4 illustrate the potential for using Kα/Kβ ratios to investigate sample heterogeneity in the depth dimension though the technique's accuracy will be dependent on the element of interest and the matrix mass absorption at Kα and Kβ fluorescence energies. Eqn. 1 can be used to examine the sensitivity of this technique for these simple two-layered systems. The ratio of Kα to Kβ fluorescence is:

$$\ln\left(\frac{I_{\mathrm{L}}'(\alpha)}{I_{\mathrm{L}}'(\beta)}\right) = \ln(S) + \left\{\rho_{\mathrm{f}}' d\left(\mu_{\mathrm{f}}'(\lambda_\beta) - \mu_{\mathrm{f}}'(\lambda_\alpha)\right)\right\} \qquad (2)$$

where $S$ accounts for the relative intensity of Kα and Kβ fluorescence originating from the fluorescing underlayer and $\rho_{\mathrm{f}}' d(\mu_{\mathrm{f}}'(\lambda_\beta) - \mu_{\mathrm{f}}'(\lambda_\alpha))$ accounts for the overlayer effect. If the difference between $\lambda_\alpha$ and $\lambda_\beta$ is very small, or if the overlayer thickness, $d$, approaches 0,

$$S \approx \frac{I_{\mathrm{L}}(\alpha)}{I_{\mathrm{L}}(\beta)} \approx \frac{I_{\mathrm{L}}'(\alpha)}{I_{\mathrm{L}}'(\beta)} \qquad (3)$$

The depth resolution can be approximated by relating the change in element depth to a detectable change in the Kα/Kβ ratio. Assuming that a 5% change in the Kα/Kβ ratio is detectable and assuming that the matrix mass absorption as a function of energy is smooth and negative between Kα and Kβ energies, then:

$$d(\text{resolvable}) = \frac{-0.05}{\rho_{\mathrm{f}}'(\mu_{\mathrm{f}}'(\lambda_\beta) - \mu_{\mathrm{f}}'(\lambda_\alpha))} \qquad (4)$$

Fig. 5 shows $\mu_{\mathrm{f}}'(\lambda_\alpha) - \mu_{\mathrm{f}}'(\lambda_\beta)$ *versus* $d$ at the densities of two minerals, hematite ($Fe_2O_3$) and calcite ($CaCO_3$). Overlain on this plot is the calculated K-shell mass absorption difference for some elements in the first transition metal series as well as Ca, Se, and Sn and the Sn L-shell mass absorption difference. Thus, for Cu in a calcite matrix, sample heterogeneity in the depth dimension could be detected at approximately 10 μm. In general, the depth resolution increases with decreasing fluorescence energy. The only exception to this trend is when the overlying matrix transitions between K-shell and L-shell (or any other shell) mass absorption. This is most evident in the depth resolution change between Mn and Cu in the $Fe_2O_3$ matrix. Since the Mn K-shell fluorescence energy, unlike Cu, is below the K-shell absorption energy for Fe, Mn K-shell fluorescence is absorbed more weakly than Cu. Nevertheless, for most first row transition metals in these light element matrices, the depth resolution varies between 3 and 25 μm (the positioning of the sample at 45° to the beam actually improves the resolution by a factor of 0.7). In addition, higher depth resolution for heavier elements may be possible by using a Lα/Lβ ratio (as shown for Sn in Fig. 4). It must be noted that no attempt was made to test the element concentration detection limit and that this additional factor will control the experimental detection limit of this technique. Nevertheless, the technique can provide improved elemental concentration quantification for 2-D elemental mapping using SXRFM.

As an example of the potential use of the fluorescence ratio method, we examined the Ca Kα, Ni Kα, and ln(Ni Kα/Ni Kβ) fluorescence data across the calcite–serpentine interface of a rock from the Panoche Valley, CA (Fig. 6). We had previously hypothesized that the gradual decrease in Ni Kα fluorescence across the boundary indicated Ni diffusion from the serpentine to calcite, particularly since the Ca Kα boundary was rather sharp.[28] There is, in fact, no way to distinguish between heterogeneity and solid state diffusion from Ni Kα data alone. The reason for this is a combination of two factors: a) the beam

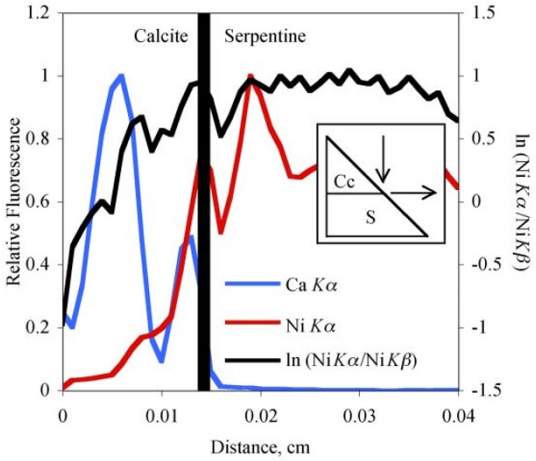


**Fig. 6** Ca Kα, Ni Kα, and ln(Ni Kα/Ni Kβ) fluorescence across the serpentine (S) calcite (Cc) boundary. Dark line is the approximate position of the interface with Ni-serpentine to the right of the line. Inset shows the orientation of the calcite–serpentine interface as determined by matching experimental results with model orientations (arrows indicate direction of primary and secondary X-rays).

angle to the sample (typically at 45°) and the beam depth of penetration results in a beam interaction *volume* much larger than the initial beam spot size and b) the particular angle of the serpentine–calcite interface in the depth dimension will influence the fluorescence signal across that interface. The ln(Ni Kα/Ni Kβ) data (Fig. 6) indicates that sample heterogeneity significantly influenced the Ni fluorescence data (average depth of Ni increased when scanning from the serpentine to the calcite as depicted in Fig. 6).

The effect of interface orientation on fluorescence results can be compared to model calculations. Assuming Ni (1500 ppm) was only found in the serpentine fraction of the sample, the fluorescence across the interface will change depending on sample orientation. By comparing the Panoche Creek sample results to predicted ln(Ni Kα/Ni Kβ) fluorescence for a variety of sample orientations, we conclude that the fluorescence data could be qualitatively explained by a calcite–serpentine interface orientation as shown in Fig. 6. Solid state diffusion is, therefore, not necessary to explain the Ni fluorescence data across the interface boundary. This result illustrates the danger of directly relating SXRFM fluorescence intensity to element concentration. It is of paramount importance that the potential for heterogeneity effects be accounted for when quantifying element concentrations; the fluorescence ratio method can, in some cases, be used to help interpret the SXRFM results. In Fig. 6, fluorescence data are shown for Ni and Ca along with ln(Ni Kα/Ni Kβ). Other transition elements could show a similar trend as Ni, *i.e.*, if Co were present in high enough concentrations in the serpentine, it should also show the "apparent" diffusion into calcite. But, when corrected for depth, it would result in the same interpretation as for Ni.

## Conclusions

The difference in calcite mass absorption at Cu Kα and Kβ fluorescence energies, coupled with a focused synchrotron beam, was used to resolve the position of Cu to a 2 × 2 × 10 ($x$, $y$, $z$, where $z$ is the depth coordinate) micrometer scale in a simple layered system. This technique could be used for a variety of elements. The resolution is dependent on the fluorescing element and the nature of the matrix material. For the first transition metal series elements in a calcite or iron oxide matrix, the depth resolution will fall in the 10–25 μm range. For complex heterogeneous systems, determination of average element depth may be computationally limited. The technique can, nevertheless, be used to investigate heterogeneity effects; we showed that the steady decrease of Ni across a calcite–serpentine boundary could be explained equally well by sample heterogeneity instead of Ni diffusion into calcite. Depth heterogeneity in samples can lead to misinterpretation of synchrotron X-ray microprobe results unless care is taken to account for the influence of heterogeneity on fluorescence data.


## Acknowledgements

Courendlin limestone was donated by Rudy Wenk of the Geology and Geophysics Department, U.C. Berkeley. Limestone wedges were constructed with the help of Tim Teague and John Donovan of the Geology and Geophysics Department, U.C. Berkeley. Karen Chapman and Albert C. Thompson helped run samples at the ALS microprobe beam line 10.3.1. Patt Nuessle ran Sn and Cu wedges at the NSLS beam line X26A. We also wish to thank Tetsu K. Tokunaga for helpful suggestions and draft review. Research was supported by the Lawrence Berkeley National Laboratory, Laboratory Directed Research and Development Program and the Kearney Foundation of Soil Science. This work was performed under the auspices of the US Department of Energy by the University of California, Lawrence Livermore National Laboratory under contract no. W-7405-Eng-48.


## Appendix

### Fluorescence from a homogeneous sample

For this derivation, the orientation of the primary beam ($I_0$), exiting fluorescence beam ($I_1$), and sample geometry are as shown in Fig. 7. The equations are derived for monochromatic source radiation although the source type will not affect the results of the fluorescence ratio technique. Secondary fluorescence and beam scattering are also ignored in this derivation.

**A close-up view of (1) a homogeneous sample and its interaction with the beam and (2) a simple heterogeneous sample.**

The change in primary X-ray intensity as it travels through a short length of sample (labeled d$x$ in Fig. 7) can be described by:

$$\mathrm{d}I(\lambda_\mathrm{p}) = -\rho_\mathrm{f}\mu_\mathrm{f}(\lambda_\mathrm{p})I(\lambda_\mathrm{p},x)\mathrm{d}x \qquad \text{(a1)}$$

where: $\mathrm{d}I(\lambda_\mathrm{p})$ is the change in intensity of primary energy ($\mathrm{cm}^{-2}$); $\mu_\mathrm{f}(\lambda_\mathrm{p})$ is the *sample* mass absorption coefficient at primary energy ($\mathrm{cm}^2\ \mathrm{g}^{-1}$); $\rho_\mathrm{f}$ is the density of sample ($\mathrm{g\ cm}^{-3}$); and $I(\lambda_\mathrm{p},x)$ is the intensity of primary energy at depth $x$ ($\mathrm{cm}^{-2}$). The sample mass absorption coefficient at the primary X-ray energy, $\mu_\mathrm{f}(\lambda_\mathrm{p})$, is

$$\mu_\mathrm{f}(\lambda_\mathrm{p}) = \sum_1^n C_i\mu_i(\lambda_p) \qquad \text{(a2)}$$

where: $\mu_i(\lambda_\mathrm{p})$ is the mass absorption coefficient of element $i$ at the primary energy ($\mathrm{cm}^2\ \mathrm{g}^{-1}$); $C_i$ is the concentration of element $i$ with respect to mass ($\mathrm{g\ g}^{-1}$); and $n$ is the number of elements. The intensity of the primary energy at depth $x$ in the

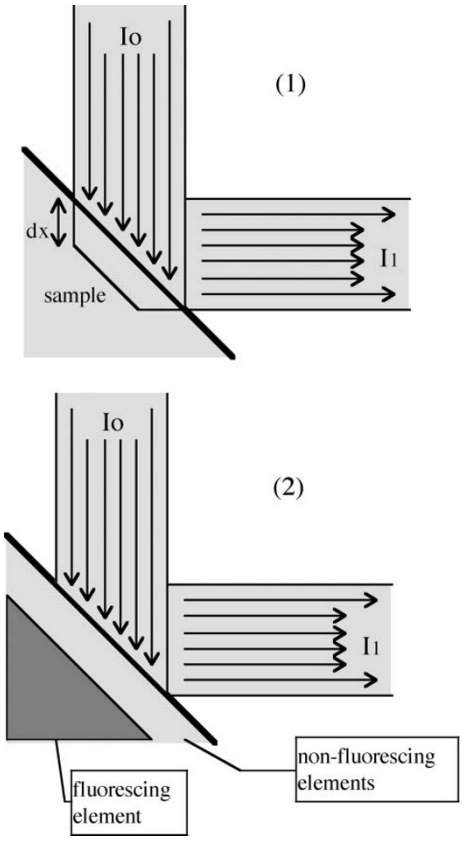


**Fig. 7** A close-up view of (1) a homogeneous sample and its interaction with the beam and (2) a simple heterogeneous sample.

sample, $I(\lambda_p,x)$, can be calculated from Beer's law:

$$I(\lambda_p,x) = I_o(\lambda_p)e^{-\rho_f x \mu_f(\lambda_p)} \quad \text{(a3)}$$

where $I_0(\lambda_p)$ is the primary intensity per area ($cm^{-2}$). The local secondary beam or fluorescence beam, $I(\lambda_s)$, will be a function of the local intensity of the primary energy, the fluorescence yield, and the fraction of absorption due to the fluorescing compound:

$$dI_x(\lambda_s) = \frac{kC_e\mu_e(\lambda_p)}{\mu_f(\lambda_p)} dI(\lambda_p) \quad \text{(a4)}$$

where: $k$ is the fluorescence yield; $C_e$ is the concentration of the fluorescing element (g $g^{-1}$); and $\mu_e(\lambda_p)$ is the mass absorption coefficient of fluorescing element ($cm^2$ $g^{-1}$). The actual fluorescence intensity that reaches the surface of the sample will be a function of the distance from the point of fluorescence to the surface by way of Beer's law:

$$dI_L(\lambda_s) = e^{-\rho_f x \mu_f(\lambda_s)} dI_x(\lambda_s) \quad \text{(a5)}$$

Eqns. a1–a5 can be combined to form:

$$dI_L(\lambda_s) = kC_e\rho_f I_0(\lambda_p)\mu_e(\lambda_p)e^{-\rho_f x(\mu_f(\lambda_s)+\mu_f(\lambda_p))}dx \quad \text{(a6)}$$

which can be integrated with respect to the sample parameters (integrated from 0 to $L$):

$$I_L(\lambda_s) = kC_e I_0(\lambda_p)\mu_e(\lambda_p)\{1-e^{-\rho_f L(\mu_f(\lambda_p)+\mu_f(\lambda_s))}\} \quad \text{(a7)}$$

where $0.707L$ is the thickness of the sample (cm). Note that the sample is effectively infinitely thick when $L > 5(\rho_f(\mu_f(\lambda_p) + \mu_f(\lambda_s)))^{-1}$.

### Fluorescence from a simple heterogeneous sample

Fig. 7 presents a very simple 2-D sample which is heterogeneous with respect to sample depth dimension. In this case, the primary X-ray intensity loss and the secondary fluorescence X-ray intensity loss due to the overlying non-fluorescing portion of the sample must be added to eqn. a7. The loss of fluorescence intensity can be taken into account by adding a Beer's Law factor for the primary energy loss and another for secondary energy loss. Eqn. a7 then becomes:

$$I'_L(\lambda_s) = I_L(\lambda_s)e^{-\rho'_f d(\mu'_f(\lambda_p)+\mu'_f(\lambda_s))} \quad \text{(a8)}$$

where: $\mu'$ is the mass absorption of the non-fluorescing overlayer ($cm^2$ $g^{-1}$); $\rho'$ is the density of the overlayer (g $cm^{-3}$); $d$ is the thickness of the overlayer (cm); $I'_L(\lambda_s)$ is the fluorescence intensity from the heterogeneous sample ($cm^{-2}$); and $I_L(\lambda_s)$ is eqn. a7 calculated for the fluorescing layer of the sample ($cm^{-2}$).

## References


1 M. L. Rivers, S. R. Sutton and J. V. Smith, *Fortschr. Mineral.*, 1988, **66**, 135.
2 J. H. Underwood, *Rev. Sci. Instrum.*, 1986, **57**, 2119.
3 J. H. Underwood, J. T. W. Berbee and C. Frieber, *Appl. Opt.*, 1986, **25**, 1730.
4 C. J. Sparks and G. E. Ice, *Mater. Res. Soc. Proc.*, 1989, **143**, 223.
5 J. V. Smith, M. L. Rivers, S. R. Sutton and K. W. Jones, *Geol. Soc. Am.-Abstracts*, 1987, **19**, 849.
6 S. Bajt, S. R Sutton and J. S. Delaney, *Geochim. Cosmochim. Acta*, 1994, **58**, 5209.
7 P. J. Potts, F. W. Bowles, S. J. B. Reed and M. R. Cave, *Microprobe Techniques in the Earth Sciences*, Chapman & Hall: London, 1995, p. 419.
8 T. K. Tokunaga, S. R. Sutton and S. Bajt, *Soil Sci.*, 1994, **158**, 421.
9 F. Bernstein, *Adv. X-Ray Anal.*, 1963, **6**, 436.
10 P. F. Berry, T. Futura and J. R. Rhodes, *Adv. X-Ray Anal.*, 1969, **12**, 612.
11 G. W. Brindley, *Philos. Mag.*, 1945, **36**, 347.
12 F. Claisse and C. Samson, *Adv. X-Ray Anal.*, 1962, **5**, 335.
13 C. B. Hunter and J. R. Rhodes, *X-Ray Spectrosc.*, 1972, **1**, 107.
14 A. Kuczumow, Z. Rzaczynska and M. Szewczak, *X-Ray Spectrosc.*, 1982, **11**, 135.
15 M. Lankosz, *X-Ray Spectrosc.*, 1993, **22**, 125.
16 J. R. Rhodes and C. B. Hunter, *X-Ray Spectrosc.*, 1972, **1**, 113.
17 J. L. de Vries and B. A. R. Vrebos, Quantification by XRF Analysis of Infinitely Thick Samples in *Handbook of X-Ray Spectrometry*, R. E. van Grieken and A. A. Markowicz, eds., Marcel Dekker, Inc., New York, 1992, pp. 312–337.
18 A. A. Markowicz and R. E. van Grieken, Quantification in XRF Analysis of Intermediate-Thickness Samples in *Handbook of X-Ray Spectrometry*, R. E. van Grieken and A. A. Markowicz, eds., Marcel Dekker, Inc., New York, 1992, pp. 339–357.
19 R. D. Giauque, J. M. Jaklevic and A. C. Thompson, *Anal. Chem.*, 1986, **58**, 940.
20 A. Markowicz, *X-Ray Spectrosc.*, 1983, **12**, 134.
21 B. Holynska and A. Markowicz, *X-Ray Spectrosc.*, 1981, **10**, 61.
22 B. Holynska and A. Markowicz, *X-Ray Spectrosc.*, 1982, **11**, 117.
23 M. L. Rivers, S. R. Sutton and J. V. Smith, *Chem. Geol.*, 1988, **70**, 179.
24 M. L. Rivers, S. R. Sutton, J. V. Smith and K. W. Jones, *Geol. Soc. Am.-Abstracts*, 1987, **19**, 821.
25 C. J. Sparks Jr., X-Ray Fluorescence Microprobe for Elemental Analysis in *Synchrotron Radiation Research*, H. Winick and S. Doniach, eds., Plenum Press, New York, 1980, pp. 459–511.
26 P. Philippot, B. Menez, P. Chevallier, F. Gibert, F. Legrand and P. Populus, *Chem. Geol.*, 1998, **144**, 121.
27 S. R. Sutton, M. L. Rivers, S. Bajt and K. W. Jones, *Nucl. Instrum. Methods Phys. Res., Sect. B*, 1993, **75**, 553.
28 H. E. Doner and M. Zavarin, The Role of Soil Carbonates in Trace and Minor Element Chemistry in *Soils and Environment - Soil Processes from Mineral to Landscape Scale*, K. Auerswald, H. Stanjek and J. M. Bigham, eds., Catena Verlag, Weinheim, 1996, pp. 407–422.
29 J. Wernisch, C. Pohn, W. Hanke and H. Ebel, *X-Ray Spectrosc.*, 1984, **13**, 180.
30 W. H. McMaster, N. K. D. Grande, J. H. Mallett and J. H. Hubbell, *Compilation of X-Ray Cross Sections*, Lawrence Radiation Laboratory, University of California, 1969.